Influence of Van der Waals Forces on Elastic and Buckling Characteristics of Vertically Aligned Carbon Nanotubes

Aparna Gangele, Sathish Kumar Garala, Ashok Kumar Pandey

PII: S0020-7403(18)31645-X
DOI: https://doi.org/10.1016/j.ijmecsci.2018.07.032
Reference: MS 4444

To appear in: *International Journal of Mechanical Sciences*

Received date: 22 May 2018
Revised date: 10 July 2018
Accepted date: 24 July 2018

Please cite this article as: Aparna Gangele, Sathish Kumar Garala, Ashok Kumar Pandey, Influence of Van der Waals Forces on Elastic and Buckling Characteristics of Vertically Aligned Carbon Nanotubes, *International Journal of Mechanical Sciences* (2018), doi: https://doi.org/10.1016/j.ijmecsci.2018.07.032

Highlights

- FEM based model with and without van der Waals interaction is developed and validated for SWCNTs and DWCNTs.
- FEM modeling of VACNTs with and without van der Waals forces are presented.
- Influence of arrays size of VACNTs on elastic modulus is studied.
- Influence of arrays size, intertube spacing and tube diameter on buckling strength of VACNTs is studied.

Influence of Van der Waals Forces on Elastic and Buckling Characteristics of Vertically Aligned Carbon Nanotubes

Aparna Gangele, Sathish Kumar Garala and Ashok Kumar Pandey*

Department of Mechanical and Aerospace Engineering, Indian Institute of Technology Hyderabad, Kandi, Sangareddy 502285, India.

Abstract

Vertically aligned carbon nanotubes (VACNTs) have been explored widely in various applications due to their unique anisotropic properties. However, its application is limited due to large aspect ratio of nanotubes which lead to buckling phenomena. In this paper, we perform a finite element analysis to predict the variation of elastic modulus and critical buckling load of VACNTs. While elastic modulus is obtained from the slope of stress-strain variation of tubes when one end is fixed and another end is subjected to longitudinal loading, critical buckling load is found using eigenvalue analysis corresponding to first buckling mode. We also perform study to show size dependence of elastic modulus and buckling load of single walled carbon nanotubes (SWCNTs) using FEM approach and compare the results with MD results found in the literature. After validating FEM approach with available results of single-walled and double-walled carbon nanotubes, we apply the same method to arrays of VACNTs. It is found that elastic modulus of VACNTs increases from 1.18 TPa to 2.02 TPa when the size increases from 4 to 36 tubes and then it becomes nearly size independent. The variations of critical buckling load versus other parameters such as tube diameter, intertube spacing, etc., are also obtained. It is found that with the increase in diameter, there is a steep rise in the buckling load for the case of VACNTs arrays. In order to show the influence of non-linear van der Waals force in VACNTs, we compare the above results with and without the presence of van der Waals force and discuss its significance. The modelling and analysis presented in the paper can be used to optimise the number density of VACNTs for different applications.

Keywords: Vertically aligned carbon nanotube arrays, Single-walled carbon nanotube, van der Waals interaction, Finite element method, Elastic modulus, Buckling.

1. Introduction

Carbon nanotubes (CNTs) have been the subject of intense research in various fields ranging from aerospace to biomedical application due to their excellent mechanical, thermal and electrical properties

*Corresponding author

Email address: ashok@iith.ac.in (Aparna Gangele, Sathish Kumar Garala and Ashok Kumar Pandey)

[1, 2]. Among many forms of the CNTs, vertically grown CNTs which are used for current or voltage related devices have been explored widely due to their unique anisotropic properties [3]. However, due to their slender length, CNTs are limited by the buckling phenomena. To overcome this limitation, the researchers started focusing on vertically aligned carbon nanotubes (VACNTs) of different densities. VACNT arrays which are studied in the form of brushes, forests, films, mats and turf are characterized by the CNTs orientation, density and intertube distance [4, 5, 6, 7, 8].

To theoretically understand the behavior of VACNTs, many researchers have developed different computational methods [9, 10, 11, 12]. Buckling behavior [13, 14] which involves large deformation requires nonlinear modeling. Ru et al. [15] analyzed the buckling of multiwalled carbon nanotubes (MWCNT) reinforced elastic medium under the influence of van der Waals forces using an elastic model. Buehler et al. [16] studied the deformation mechanism of very long SWCNTs under compressive buckling load. They specified a shell-rod-wire transition of the mechanical behaviour of CNTs with increasing aspect ratios. Li et al. [17] observed the unique local buckling behavior of VACNT arrays considering the van der Waals interaction only as lateral support and its propagation using the finite element method. Yakobson et al. [18] evaluated and compared the results of molecular dynamics and continuum shell model for buckling of CNTs and inferred that the continuum model provides a remarkably accurate roadmap of nanotube behavior beyond Hooke's law if model parameters are properly taken. Ru [19, 20] employed a classical continuum shell model enabling the van der Waals interlayer interactions to study the buckling of SWCNTs and MWCNTs under axial compression and external pressure. Li et al. [12] used the molecular structural mechanics approach for modeling the elastic buckling of SWCNTs and MWCNTs under bending and axial compression. Zhang and Shen [21] analysed the thermal buckling of initially compressed SWCNTs subjected to a uniform temperature rise using the MD simulations. Murmu and Pradhan [22] used the nonlocal elasticity and Timoshenko beam theory to estimate the stability response of SWCNT embedded in an elastic medium. Guo et al. [23] employed the atomic-scale FEM to estimate bending buckling of SWNTs. Yao et al. [24] have performed extensive FEM simulations to demonstrate the buckling behavior of SWCNTs and MWCNTs under bending deformation. They found that the FEM-based results agree well with that from atomistic methods and can reduce the computational cost of atomistic models mainly for large-scale CNTs and systems having a large number of CNTs. To the best of authors' knowledge, the numerical analysis of VACNT arrays including nonlinear van der Waals interactions, which provides for the lateral and oblique support along the length of adjacent tubes, is not yet done. Their inclusion is needed to provide a more realistic numerical model for VACNT arrays.

In this paper, we present a systematic numerical model for arrays of VACNTs to analyze the influence of arrays parameters on their elastic modulus and buckling load. After validating the numerical model, we perform simulations to obtain the stress-strain curves for arrays of VACNTs to observe the influence of arrays parameter on elastic modulus. We then compute the critical buckling load in arrays of CNTs

and analyze its dependence on tube diameter, configuration (armchair or zigzag) and arrays density. The chirality, diameter, aspect ratio and intertube spacing to model the arrays are selected based on the studies performed on different SWCNTs in the present work. All the above studies are performed with and without non-linear van der Waals interaction force to show its significance in the modeling of VACNTs arrays.

2. Numerical implementation based on finite element modeling

To perform the numerical analysis, CNTs are replaced by an equivalent structural model. For this, the carbon atoms connected by a covalent bond of fixed characteristic length are replaced by load-bearing beam elements connecting the nodes [11]. Molecular mechanics and structural mechanics models are correlated to get the equivalent model. The corresponding structural model is used to evaluate the different mechanical properties using FEM. The equivalent properties of beam based on carbon-carbon bond is obtained by comparing the equivalent energy based on molecular and structural mechanics approaches [25]. Table 1 presents the relationship among different parameters of circular beam element of diameter (d), length (L), the Young's modulus (E) and the shear modulus (G).

Here, the length of beam element, L, is taken as the bond length of C–C bond which is 0.142 nm; and k_r, k_θ, and k_τ are the spring coefficients of covalent bond in tension, bending and torsion, respectively, and their values for taken as 653 nN/nm, 0.879 nN-nm/rad^2 and 0.278 nN/rad^2, respectively [11, 26, 27, 28]. ΔL, $\Delta\alpha$ and $\Delta\beta$ are the deformations under tension, bending and torsion, respectively. $A = \pi d^2/4$ is cross-sectional area of the beam; $I = \pi d^4/64$ and $J = \pi d^4/32$ are cartesian and polar moments of inertia for the circular cross-section of beam, respectively. Thus, the final properties for beam element to be used in FEM are taken as $d = 0.147$ nm, $E = 5488$ nN/nm^2, $G = 871.1$ nN/nm^2, and Poisson's ratio as 0.3, respectively [26].

Table 1: Relation derived from Chemical and Mechanical Parameters

	Covalent bond Energy	Strain energy of Beam	Relation after equating
Tension	$\frac{1}{2}k_r(\Delta r)^2$	$\frac{1}{2}\frac{EA}{L}(\Delta L)^2$	$d_o = 4\sqrt{\frac{k_\theta}{k_r}}$
Bending	$\frac{1}{2}k_\theta(\Delta\theta)^2$	$\frac{1}{2}\frac{EI}{L}(\Delta\alpha)^2$	$E = \frac{L(k_r)^2}{4\pi k_\theta}$
Torsion	$\frac{1}{2}k_\tau(\Delta\phi)^2$	$\frac{1}{2}\frac{GJ}{L}(\Delta\beta)^2$	$G = \frac{L(k_r^2 k_\phi)}{8\pi k_\tau^2}$

2.1. Modeling of Nanotubes in FEM

In this section, we describe the method of modeling carbon nanotubes using FEM in ANSYS. To model CNTs, carbon atoms are represented as structural masses or joints, and chemical bonds between the atoms are represented as beams, rods, trusses or springs, etc. [11] forming a space frame structure. To model SWCNTs or DWCNTs arrays, two types of bonds, namely, the covalent bond and non-covalent bond due to

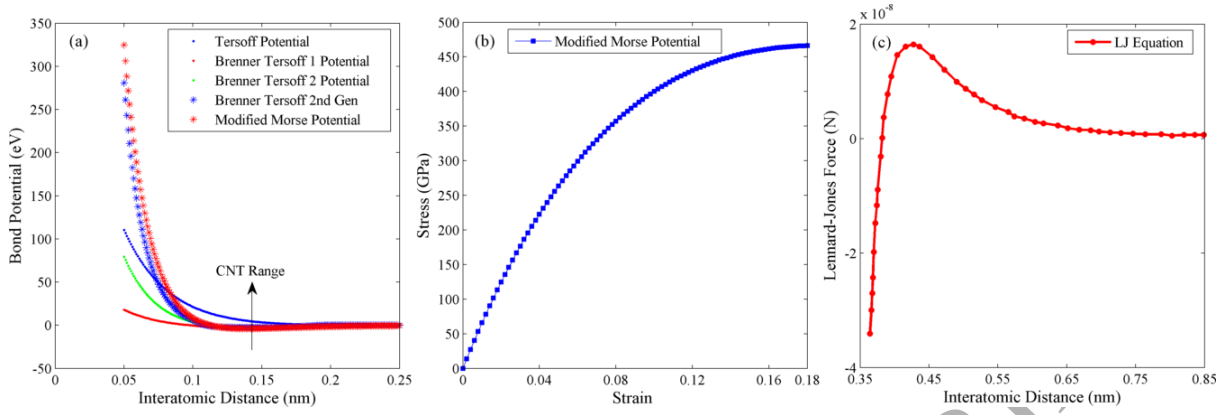

Figure 1: (a) Plot of different bond potentials with interatomic distance for C-C covalent bond. (b) The tensile stress-strain correlation for beam elements obtained from modified Morse potential, used to model the covalent bonds between carbon atoms. (c) The load-displacement correlation for nonlinear spring elements derived from Lennard-Jones potential used to model van der Waals force. The x-axis represents the length of a spring element (nm) while the y-axis represents the load on a spring element (N).

van der Waals interaction, are considered as mechanical element. The precision of this numerical analysis mainly depends on the accuracy of the selected interatomic and intermolecular potentials energy functions. These potentials are broadly used in the computational analysis of nanostructures. There are many interatomic potential models available for different classes of materials. As we are dealing with CNTs in our current study, for C-C covalent bond, the interatomic potentials such as Tersoff many-body potential model, Brenner-Tersoff first generation hydrocarbon potentials, Brenner-Tersoff second-generation hydrocarbon potentials, Modified Morse potential can be considered. A comparison of all these potential models ranging from 0.05 nm to 2.5 nm of interatomic distance is represented in Figure 1(a). It can be noted from Figure 1(a) that Brenner-Tersoff second-generation potential is very close to the Modified Morse Potential which can easily be applied and is popular used by other researchers [11, 28] for performing FEM simulation. Therefore, in this work, a pairwise modified Morse interatomic potential is used to model C-C bonds.

In the present study, CNTs of desired configuration are generated through Matlab programming [29]. The coordinates of CNTs are transferred to ANSYS. The positions of each carbon atoms are located at the nodes. The covalent bonds between atoms are modeled using beam element, and the van der Waals bonds are modeled using the spring element, respectively. The van der Waals forces between two carbon atoms are highly nonlinear. Therefore, nonlinear spring elements are employed to connect the atoms. In ANSYS [30], three-dimensional Beam 188 elements are used for covalent bonds. This element is suitable for linear and nonlinear, large rotation analysis and has the potential for uniaxial tension or compression with bending and torsional deformations. The nonlinear effect can be captured effectively with NLGEOM, ON option. However, the non-linear element properties need to be defined into ANSYS for this element

in the form of material properties. The multilinear beam element property is taken from the nonlinear stress-strain diagram as shown in Figure 1(b). Additionally, the elastic modulus which represents the slope of linear variation of stress versus strain at low strains is also defined. The nonlinear spring element is used to model non-covalent bonds which is suitable for uniaxial tension and compression. These elements are defined by two nodes and a nonlinear force-displacement relation obtained by Lennard-Jones (L-J) potential as shown in Figure 1(c). Thus, the covalent bonds in SWCNTs are modelled by modified Morse potential and the non-covalent van der Waals force interactions between two consecutive SWCNTs are modelled by L-J potential. In this work, the non-linearity is due to non-linear relation caused by non-linear material properties arising from modified Morse potential between C-C atoms and the nonlinear force-displacement relation obtained by Lennard-Jones (L-J) potential in modelling arrays of VACNTs.

2.1.1. Single-walled carbon nanotubes

In this section, we follow above mentioned approach to model SWCNT. To do the analysis, the tube thickness is taken as 0.34 nm which is same as the van der Waals diameter of carbon [12]. One end of the tube is fixed and another end is displaced longitudinally by ΔL gradually. For a given displacement, the reaction force, F_{net}, at the fixed end is computed. Subsequently, the stress and strain are computed and plotted. Finally, the elastic modulus, E, is found as the ratio of stress versus strain using the following relation

$$E = \frac{\sigma}{\varepsilon} = \frac{\frac{F_{\text{net}}}{A_0}}{\frac{\Delta L}{L_0}} \tag{1}$$

where, $A_0 = \pi D_n t$ is the cross-sectional area of the tube and L_0 is the initial length. The comparison between computed values and available results are done in section (4).

2.1.2. Multi-walled carbon nanotubes

To validate the modeling of van der Waals forces, we model multi-walled carbon nanotubes, i.e., MWCNT, in which multiple concentric SWCNTs are placed together. In order to provide the connection between different concentric tubes, we capture van der Waals interaction through nonlinear spring element based on the Lennard-Jones or "6-12" potential [28, 31]. Figure 2 shows a typical FEM model of DWCNT. The expression of spring force based on Lennard Jones potential can be written as the negative gradient of potential as

$$F(r) = -\frac{dU(r)}{dr} = 24\frac{\epsilon}{\sigma}\left[2\left(\frac{\sigma}{r}\right)^{13} - \left(\frac{\sigma}{r}\right)^{7}\right] \tag{2}$$

where, r is the distance between interacting atoms, and ϵ and σ are the Lennard-Jones parameters. For carbon atoms, these parameters are potential well depth, $\epsilon = 0.0556$ kcal/mol $= 3.86 \times 10^{-3}$ N-nm and zero potential diameter, σ= 0.34 nm [31]. In MWCNT, an atom in one layer forms an interacting pair with many atoms from the neighbouring layers where the distance between the pair of atoms is less than 2.5σ. Therefore, van der Waals force evaluated from the Lennard-Jones potential is negligible beyond the distance

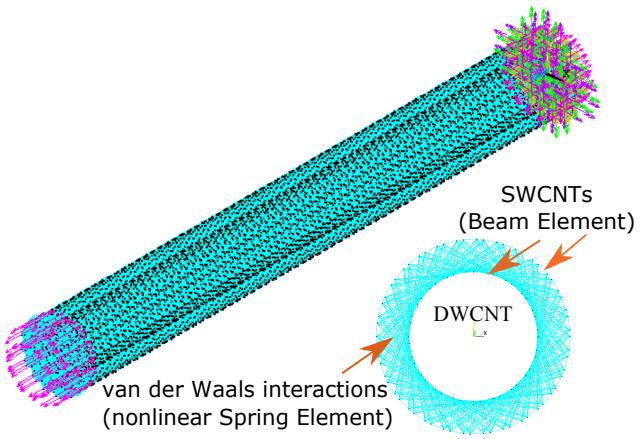

Figure 2: Schematic of typical DWCNT geometry showing covalent bonds with van der Waals bonds.

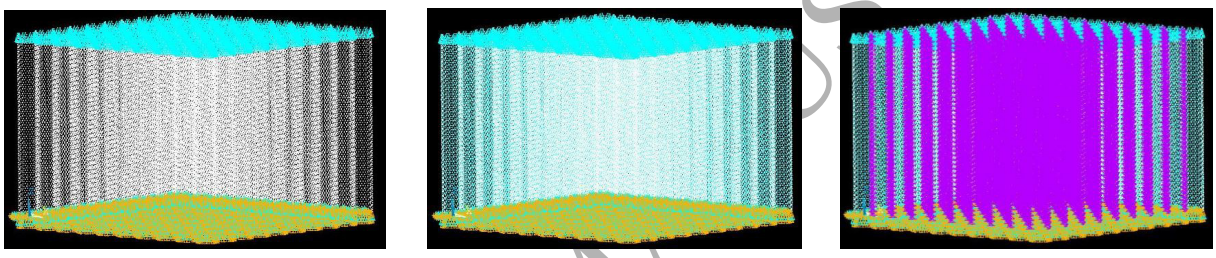

Figure 3: (a) Nodes of 10 X 10 arrays of (8,8) SWCNT with boundary conditions. (b) Beam elements of 10×10 arrays of (8,8) SWCNT with loading. (c) Connecting spring elements of 10×10 arrays of (8,8) SWCNT with loading.

2.5σ between the carbon atoms [31]. So, the connecting element is activated when the distance between two atoms located at consecutive neighbouring tubes is lesser than 2.5σ. DWCNTs with different chiralities are also investigated with axial loading and boundary conditions similar to that applied in SWCNTs as shown in Figure 2. Additionally, to obtain stress versus strain curve to compute elastic modulus using Eq. 1, we take the expression of area as,

$$A = \frac{\pi}{4}\left[(d_o + t)^2 - (d_i - t)^2\right] \tag{3}$$

where, d_o and d_i are the outer and inner diameters of the tube. The thickness, t, of each tube is taken as 0.34 nm.

2.1.3. Arrays of single-walled carbon nanotubes

In this section, we describe the modeling procedure of an array of VACNTs. Unlike, the single element of SWCNT or DWCNT, VACNTs consist of arrays of SWCNTs or DWCNTs in different patterns. Therefore, to model the influence of adjacent tubes on any other tube, non-bonding van der Waals forces are again modeled using non-linear spring element which provides lateral as well as oblique support in the radial

direction throughout the length of the adjacent tubes. Subsequently, the static analysis is done to compute elastic modulus of VACNTs. Using the computed elastic modulus of VACNTs, we perform buckling analysis to find the critical loads for fixed-free boundary condition.

To describe the modeling procedure, we take vertically aligned tubes of SWCNTs with identical chirality, diameter and length under the influence of van der Waals interactions which is captured using the non-linear spring element. We consider arrays of 4 (2×2), 16 (4×4), 36 (6×6), 64 (8×8) and 100 (10×10) SWCNTs for the study. The intertube distance between the two SWCNTs are taken as 0.34 nm, the reason for this is explained later in Sec. 4.3.1. The nanotubes are constrained at the bottom nodes and axial displacement is provided at the top nodes of all the tubes of an array as shown in Figure 3 (a). The geometries showing covalent and van der Waals bonds in case of 10×10 array of (8,8) type in Figure 3 (b) and Figure 3 (c), respectively. The thickness (t) of the nanotubes is taken as 0.34 nm. The total cross-sectional area is found by multiplying the number of tubes with the cross-sectional area of the single tube, i.e., $\pi D t$, where, D is the diameter of one SWCNT in the array. Subsequently, the stress-strain relation is found to compute the elastic modulus of VACNT arrays. Finally, we perform simulations on arrays of SWCNTs with different size to study its influence on elastic modulus.

3. Buckling Behavior

The buckling phenomena represent structural instability for a long column of a beam under compressive loading. Under this condition, the long column shows sudden and large sideways deflection due to increase in the load beyond its certain value. The load at which the buckling phenomena initiate buckling instability is called critical load. Hence, it is an important quantity to be evaluated for slender elements such as vertically aligned carbon nanotubes. The critical buckling load can be evaluated using different methods based on the theory of structural stability [32]. One of the simplest methods is based on eigenvalue or bifurcation analysis under which the structure is assumed to be an ideally elastic [12]. For fixed boundary condition at one end and compressive load or displacement at another end, the eigenvalue analysis gives critical buckling loads corresponding to different buckling modes. In general, the critical loads obtained using this method over-predicts the actual values as compared to nonlinear buckling analysis [12, 33]. In nonlinear buckling analysis, the nonlinear analysis is done in which the compressive loads are increased in small step till the buckling is observed. However, in the present paper, we use eigenvalue method to compute buckling loads in single as well as an array of VACNTs.

The critical buckling load of a slender column under compressive loading can also be obtained using the classical Euler's column buckling model [34] by various researchers [16, 35, 36, 37, 38]. The basic form of critical load to predict the CNT buckling can be represented as [12, 32, 39],

$$P_c = \frac{C\pi^2 EI}{L^2} \tag{4}$$

where, C depends on the end condition of the column, here, it is 0.25, E is the elastic modulus, I is the moment of inertia $\frac{\pi}{64}(D_o^4 - D_i^4)$ for the cross-section of CNT, D_o is the external diameter, D_i is the internal diameter of the hollow CNT, L is the length of tube. If $A = \frac{\pi}{4}(D_o^2 - D_i^2)$ is the area of CNT then the critical strain, ϵ_c, and critical stress, σ_c can be expressed as

$$\sigma_c = E\epsilon_c = \frac{P_c}{A}. \tag{5}$$

However, they can be applied directly to find critical load in arrays of VACNTs. In the subsequent section, we also modify the above formula based on the numerical analysis to compute critical loads in VACNTs.

4. Results and discussion

In this section, we first present the validation of FEM modelling of SWCNTs with molecular dynamics and other finite element results available in the literature. Subsequently, we analyze the variation of elastic modulus of VACNTs and then compute critical buckling loads as the size of arrays increases.

4.1. Validation

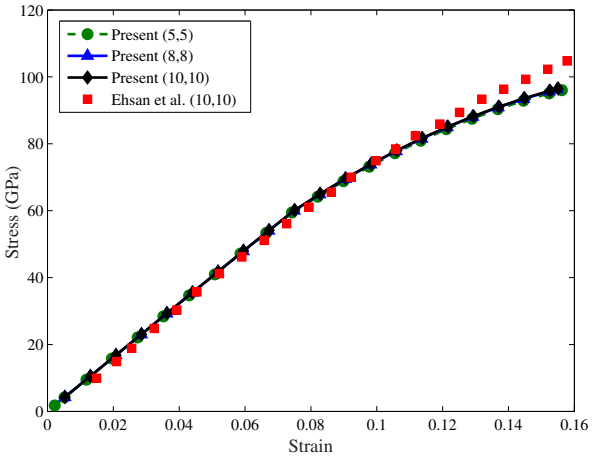

Figure 4: The nonlinear stress-strain curve for various configurations of SWCNTs.

Figure 4 and Table 2 show the validation of elastic properties of SWCNT and DWCNT (van der Waals forces). To show size dependence behavior, we have carried out further validation with MD results. Figures 5 (a) and (b) depict that for tube diameter greater than 1 nm, elastic modulus becomes nearly independent of tube diameter. On comparing the results with MD simulation, a percentage error of 8-15 % is found in case of armchair and 1.5 to 3.5% for zigzag CNTs [40]. The effect of aspect ratio of tube on the elastic property of CNT is also shown in Figure 5 (c) using different values of length ranging from 7 nm to 42.5

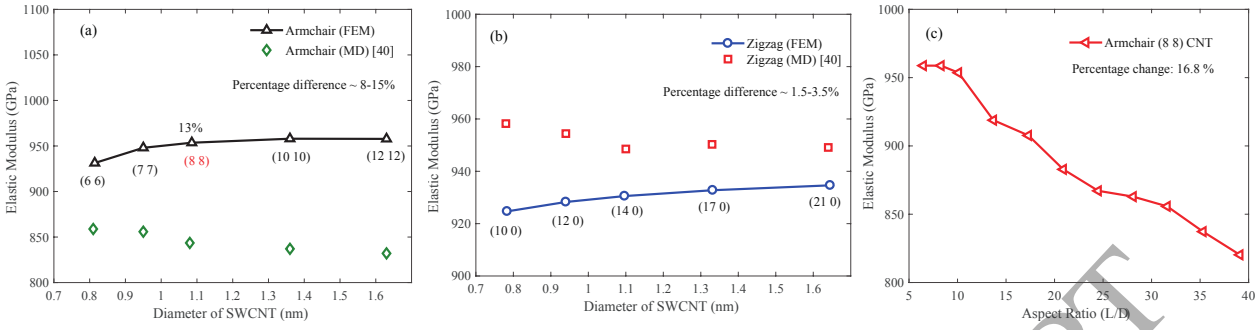

Figure 5: Comparison of the elastic modulus of the present FEM study and existing MD results[40]. Variation of elastic modulus with diameter of (a) armchair and (b) zigzag CNTs. (c) The effect of length on the elastic modulus of the (8,8) armchair SWCNT.

nm. The percentage change in elastic properties is found to be about 16% over the above range of tube length. Hence, the elastic properties also vary with aspect ratio. However, we have also found that the elastic modulus is almost constant of the aspect ratio is less than or equal to 10 which is also shown in [41]. Hence, we maintain take aspect ratio equal or less than 10 for further analysis of VACNTs.

Table 2: Young's Modulus for DWCNTs

Type of DWCNT	Young's Modulus (in TPa)	
	Ehsan et al. [28, 42]	Present Value
(5,0)-(14,0)	0.9514	0.943
(12,0)-(21,0)	0.9531	0.9728

Figure 6(a) show the comparison of critical buckling load corresponding to fundamental mode versus aspect ratio (L/D) of SWCNTs with armchair and zigzag configurations. An inset of Figure 6 (a) also show other buckling modes. Variation of critical buckling load corresponding to fundamental mode is also compared with the results obtained by Hu et al. [39] and analytical expression based on Euler buckling formula [12]. It is also found that FEM results show lower value as compared with the analytical results from Eqn. (4)[12] for lower values of aspect ratio. But it shows almost similar variation for larger aspect ratios. The same trend is observed for SWCNTs with configurations of (8,8) and (14,0) which are also compared with MD results from literature [43] as shown in shown in Figure 6 (b). It can be seen that the results are in good agreement with MD simulation results. The maximum percentage error of 18% and 15% are found in case of armchair and zigzag CNTs, respectively. Sun et al. [44] also mentioned in their work that the when the diameter of SWCNT is smaller than 1 nm and the aspect ratio is higher than 8, it will become axially unstable in the slender beam-like shape in compression. So, these two values could be considered as

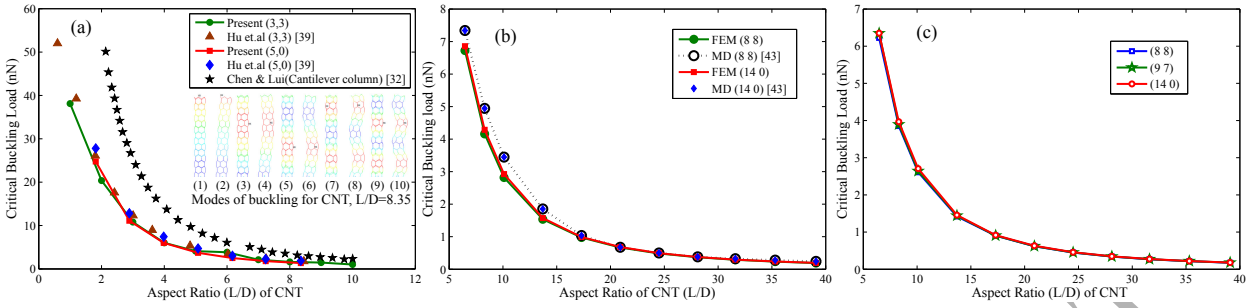

Figure 6: Comparison of the compressive critical buckling load for present and previous results obtained from different methods for SWCNT (a) armchair (3,3) and zigzag (5,0) configurations and the inset showing the various mode shapes for buckling of zigzag (5,0) CNT, L/D= 8.35, (b) Comparison of the critical compressive buckling load of the present FEM study with the existing MD simulation results [43] and (c) The influence of chirality of SWCNT on the buckling load with different aspect ratios.

critical diameter and critical aspect ratio, respectively.

To analyze the influence of chirality on the buckling property, three different configurations of SWCNTs are chosen. Maintaining the diameters of armchair (8,8), chiral (9,7) and zigzag (14,0) CNTs as 1.0856, 1.0884 and 1.0968 nm, respectively, which are nearly same, we perform buckling analysis for the range of length varying from 7.05 nm to 42.5 nm. Figure 6 (c) depicts clearly that for this range of aspect ratios, the critical buckling load is nearly identical for all the three chiral configurations. It is seen that for all the three chiral effects, the critical buckling load decreases with the increase of aspect ratio. Therefore, we would use the armchair (8,8) configurations for studying the buckling behavior of arrays of different sizes.

Additionally, the above analysis validates our methodology in which we model covalent bond between carbon atoms by beam element and non-bond van der Waals interactions using nonlinear spring element. Therefore, the same procedure can be used for performing elastic and buckling analysis in arrays of VA-SWCNTs.

4.2. Elastic behavior of VA-SWCNT arrays

To compute stress-strain curves of VA-SWCNTs, we take arrays of size 2×2, 4×4, 6×6, 8×8, and 10×10, respectively. Figure 7 shows the variation of such curves of different sizes. The variation of the slope of stress-strain curves, i.e., elastic modulus, show that it increases from 1.18 TPa to 2.02 TPa with increase in the size of arrays from $2 \times 2 = 4$ to $6 \times 6 = 36$, and then becomes stagnant at 8×8 or beyond. Such increase in elastic modulus is due to non-linear van der Waals forces between the tubes. Therefore, it can be inferred that strengthening of VACNTs by increasing the size of arrays beyond 6×6 has little effect on the elastic modulus, i.e., it shows size-independent behavior. Furthermore, an inset of Figure 7 shows that Young's modulus remains nearly unchanged if we do not consider the van der Waals interaction (i.e. no van der Waals interaction force). Now, we perform the buckling analysis of VACNTs in the next section.

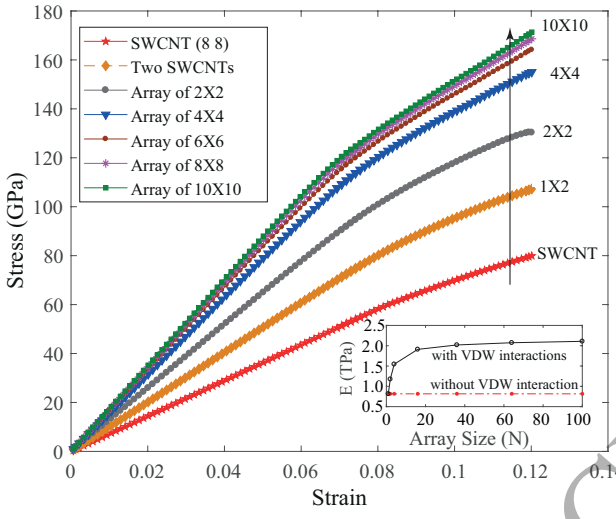

Figure 7: Nonlinear stress-strain curves for 2×2, 4×4, 6×6, 8×8 and 10×10 arrays of (8,8) SWCNTs.

4.3. Buckling behavior of VA-SWCNT arrays

In this section, we analyze the influence of intertube spacing and tube diameter on the critical buckling load of VACNTs with and without the presence of non-linear van der Waals forces.

4.3.1. Effect of intertube distance between two SWCNTs

It is observed that the spacing between two vertically aligned carbon nanotubes (VACNTs) in 1×2 array under consideration play a significant role on the overall buckling strength. Taking the minimum intertube distance as 0.34 nm based on minimum applicable distance of the L-J potential (see Eq. 2). Figure 8 show the effect of intertube distance between two SWCNTs on the critical compressive buckling load. For this purpose, the armchair (8,8) CNTs having a length of 10 nm are chosen and the range of intertube spacing is considered from 0.34-8 nm. Figure 8 depicts that the value of critical buckling load is maximum when the interlayer spacing between two VSWCNTs is 0.34 nm. An increase in interlayer spacing reduces the buckling strength due to the reduction in the strength of van der Waals forces between two VACNTs. If the non-bonded force provided by van der Waals interaction force is not considered, the buckling strength remains constant and becomes independent of intertube spacing. Since the critical buckling load is maximum at the intertube spacing of 0.34 nm, we take the same intertube spacing to study the influence of array size of VACNTs on critical buckling load.

To study the influence of array size of VACNTs on critical buckling load, the armchair (8,8) SWCNTs having diameter 1.0856 nm and tube length 5.5 nm giving an aspect ratio of approximately 5 is considered for all the arrays. Although, VACNT arrays do not always constitute purely vertical CNTs as the CNTs are entangled and somewhat hagged in shape, though, the general direction of growth is vertical. This is important for buckling studies, but for the sake of simplicity, we assume vertically aligned straight nanotubes

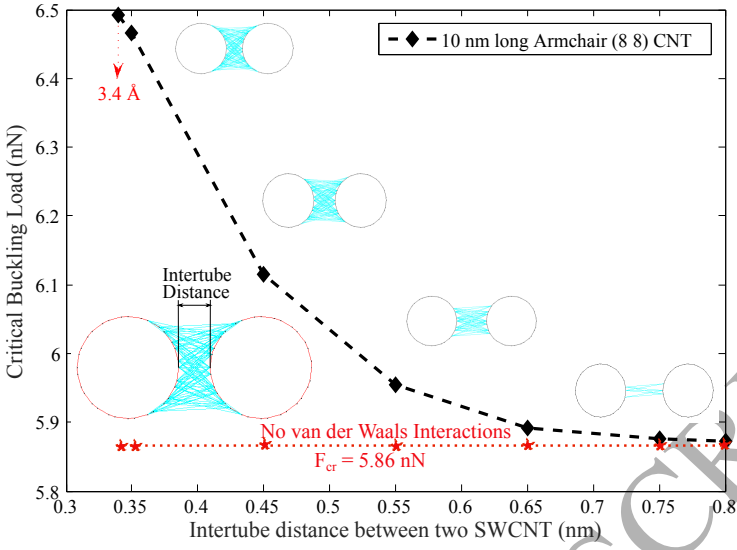

Figure 8: Variation of critical buckling load with intertube distance between two SWCNTs. The inset schematic shows that number of non covalent bonds decreases with increase in the intertube distance.

as shown in Figures 3 (a)-(c) in this analysis. For fixed boundary condition at one end and uniformly distributed compressive loading at another end, we perform buckling analysis to find critical buckling load in VA-SWCNTs arrays of different size. Figure 9 shows the first buckling mode for VA-SWCNT arrays of varying size. It is interesting to note that the deformed mode shapes under buckling are similar for varying number of tubes in arrays. Corresponding to first buckled mode, Figure 10 (a) shows that the compressive buckling load increases linearly with a number of tubes for same values of the tube length, chirality and intertube spacing in arrays. However, when the buckling load is plotted in log scale, the influence of van der Waals forces on the buckling strength of different size of arrays can be analyzed nicely. It is found that for constant length and intertube spacing between VACNTs, the buckling load increases linearly and then becomes nearly independent of array size as shown in Figure 10(a). On comparing the variation of buckling load with and without van der Waals forces, the trends found to be similar but the magnitude of buckling load is found to be lesser if van der Waals forces are not considered.

Similarly, Figure 10(b) shows the influence of tube diameter on critical buckling load for armchair as well as zigzag configurations of 8×8 VACNTs array with tube length of 5.5nm. It is observed that the buckling load first reduces significantly with tube diameter for both the configurations till the diameter of 0.54 nm before becoming constant. It is found that the diameter of 0.54 nm corresponds to the chirality of (4,4) in case of armchair and (7,0) in case of zigzag configurations, respectively. The reason for this behavior is that at the smallest diameter (i.e., (2,2) and (3,0) for armchair and zigzag, respectively), the number of van der Waals interactions is maximum An increase in diameter causes it to reduce, and, thus, the critical buckling load decreases. Later, the buckling load becomes invariable with further increases in diameter. Figure 10

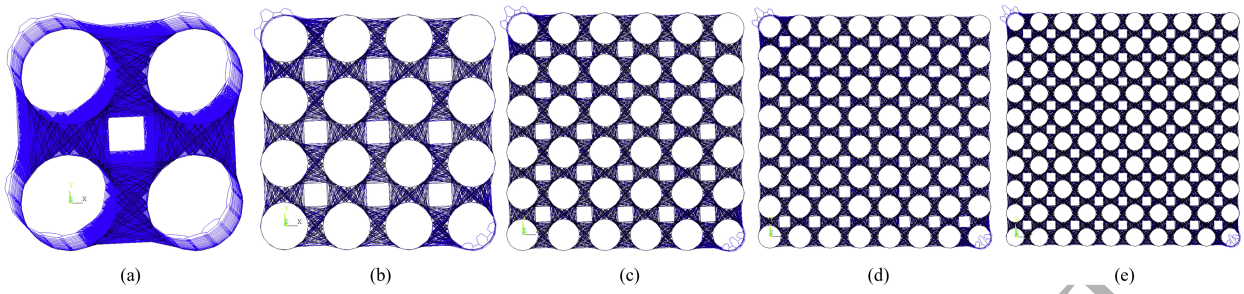

Figure 9: (a) First mode of buckling for 2×2 array, (b) 4×4 array, (c) 6×6 array, (d) 8×8 array, (e) 10×10 array of (8,8) SWCNT.

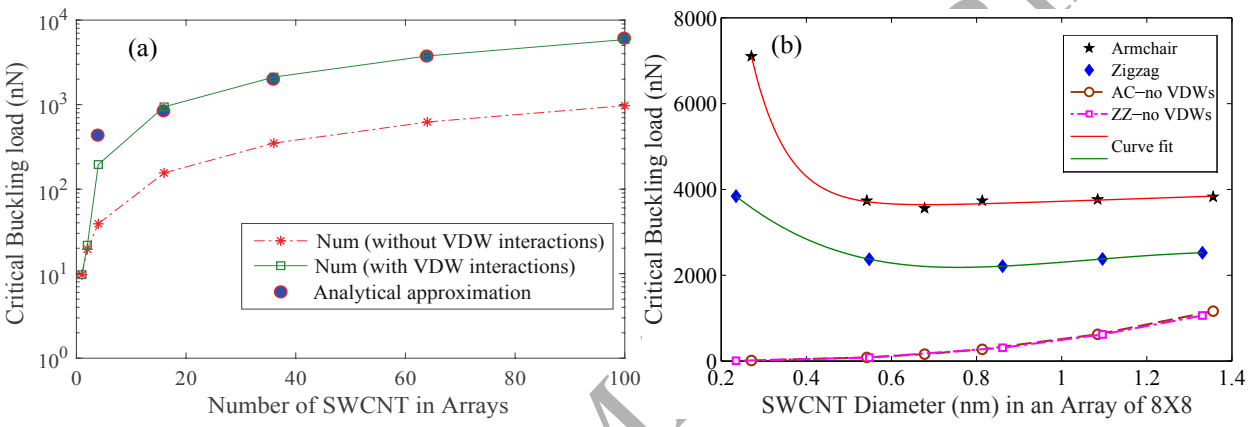

Figure 10: (a) Critical buckling load Vs Number of SWCNTs in 2×2, 4×4, 6×6, 8×8 and 10×10 arrays. Also comparison of numerical and analytical data obtained for the buckling load with number of tubes in arrays of armchair nanotubes. (b) Influence of SWCNT diameter on the buckling load for 8×8 arrays of armchair and zigzag configurations.

(b) also shows the influence of diameter of 8×8 VACNTs array on buckling load without non-linear van der Waals interactions. It shows that the critical buckling load value give smaller values (6-1000 nN) compared to the values computed without considering the van der Waals interactions. As the diameter increases, the critical load is small and remains nearly constant before increasing. However, its value remains below the buckling load obtained in the presence of van der Waals forces for the same diameter.

To develop an approximate model to compute buckling load in VA-SWCNTs, we compare the numerical solution with analytical results based on Euler's column buckling from Eqn. 4. Since the critical buckling load formula requires area moment of inertia of arrays, we compute it from the difference of rectangular cross-section of the array and the circular cross-section of tubes present in the array. The elastic modulus of different VA-SWCNTs can be taken from the inset of Figure 7. After inserting the moment of inertia, elastic modulus and the distributed load in the formula given by Eqn. (4) and comparing the results with numerical values, we obtain the modified formula as

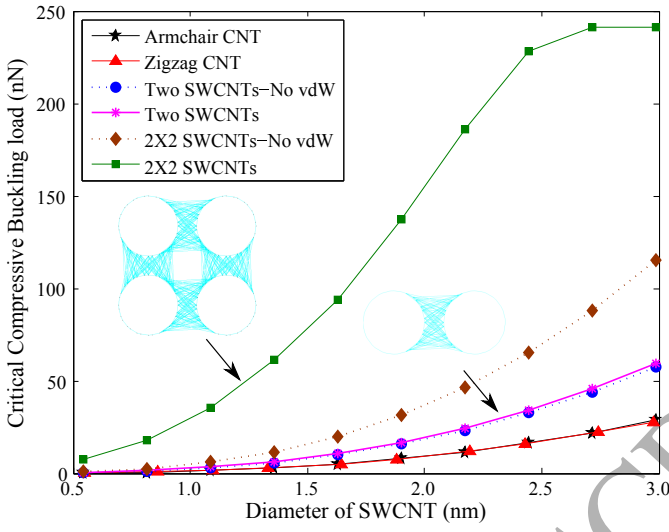

Figure 11: Comparison of critical compressive buckling load (nN) corresponding to various diameter of SWCNT ranging from 0.5 to 3 nm for armchair and zigzag configurations of SWCNTs, Two SWCNTs and 2×2 SWCNTs at the intertube distance of 0.34 nm having length of 14.2 nm.

$$P_{\mathrm{cr}}{}^{\mathrm{num}} = C_\xi \times P_{\mathrm{cr}}{}^{\mathrm{Euler}}$$

where, the correction factor is defined as (for $N > 3$),

$$C_\xi = \frac{1}{12(N-3)}, \tag{6}$$

N is the number of nanotubes in an array. Finally, the formula can be written as

$$\begin{aligned} P_{cr}{}^{num} &= \left(\frac{1}{12(N-3)}\right) \times P_{cr}{}^{Euler} \\ &= \left(\frac{1}{12(N-3)}\right) \times \left(\frac{\pi^2 EI}{4L^2}\right). \end{aligned} \tag{7}$$

Figure 10(a) shows the variation of buckling load obtained from Eqn. (7) with number of tubes, N. It captures the variation of buckling load effectively as compared with that with numerical simulation.

4.3.2. Effect of diameter of SWCNT for slander CNTs

Finally, we have also carried out a study to find the effect of diameter of a slander nanotubes of length 14.2 nm on the critical buckling load. Figure 11 demonstrates the comparison of critical compressive buckling load (nN) corresponding to various diameters of SWCNTs ranging from 0.5 to 3 nm. The SWCNTs of armchair types (4,4), (6,6), (8,8), (10,10), (12,12), (14,14), (16,16), (18,18), (20,20) and (22,22) configurations are selected. Similarly, the diameter range of zigzag type configurations (7,0), (11,0), (14,0), (17,0), (21,0), (24,0), (28,0), (31,0), (35,0) and (38,0) of SWCNTs are also considered. Two SWCNTs and 2×2 SWCNTs

are modeled for a constant intertube distance of 0.34 nm, and diameters are taken similar to that with the armchair SWCNTs. The length of all the models are fixed at 14.2 nm. It can be seen from the Figure 11 that both the armchair and zigzag types of SWCNTs show the similar buckling behavior in compression for the chosen diameter range. In case of two SWCNTs structure, the critical buckling loads are higher as compared with that of the single SWCNT. A further increases in diameter makes the curve steeper. For the case of 2×2 SWCNTs, the values of critical buckling loads increases at higher rate and then becomes independent of tube diameter. On comparing the variation of buckling load without non-linear van der Waals interaction, it is found that a significant improvement in the overall buckling strength is obtained in 2×2 array of CNTs. Whereas, no significant difference in the buckling strength of two (1×2) SWCNTs with and without van der Waals interactions is observed. Therefore, it can be inferred that with increased number of tubes the effect of non-linear van der Waals force should be considered in numerical modeling.

5. Conclusion

We have presented a finite element analysis of single as well as an array of VACNTs to analyze the influence of array parameters on the elastic modulus and critical buckling loads. To validate the modeling techniques, we first compared the results related with elastic modulus and buckling loads of SWCNT. To validate the modeling of van-der Waals forces, we compare the results of DWCNTs in which concentric tubes are modeled using this forces. After validating the modeling techniques, we apply the same method to study the influence of size, intertube spacing, and diameter of tubes on elastic and buckling characteristics with and without van der Waals forces. Taking the intertube spacing same as the minimum applicable distance of L-J potential, i.e., 0.34 nm at which the critical buckling load gives maximum value. It is found that the elastic modulus increases by about 41.6% when the array size increases from 2×2 to 6×6. Beyond this size of the array, we note that the elastic modulus becomes size-independent. Thus, it can be inferred that for the large size of the VACNT arrays, the elastic modulus becomes independent of array size and it begins to observe the classical mechanics principle. We have also shown that for aspect ratio considered in this work, the critical buckling load of SWCNT is nearly identical for different chiralities. On varying the diameter of tubes for a constant length of the armchair and zigzag SWCNTs of array size 8×8, we have found that the critical buckling load reduces sharply with increase in tube diameter. After the diameter of 0.54 nm corresponding to (4,4) armchair or (7,0) zigzag configurations, the buckling load remains almost constant. Also, it is shown that with an increase of individual CNT diameter of a slander tube of length 14.2 nm, there is a sharp increase in critical buckling load for 2×2 arrays as compared to isolated SWCNT. On comparing the above results with that of VACNTs arrays without considering non-linear van der Waals forces, we have found that van der Waals forces play an extremely important role in tuning the elastic and buckling characteristics of VACNTs. Finally, we have also proposed a modified formula to compute

buckling load in VA-SWCNT arrays which can be used to optimize the density of VACNTs for different applications. Also, this work can be considered to be an initial motivation to carry out further research in the area of numerical analysis of VACNTs which is computationally very intensive to perform using the standard method of molecular dynamic simulations.

Acknowledgement

The author AG would like to acknowledge the assistance provided by the Ministry of Human Resource Development, Government of India. We also acknowledge the discussion on the fabrication and different design aspects of VACNTs with Dr. Chandra Sekhar Sharma from IIT Hyderabad.

References

References

[1] R. Hirlekar, M. Yamagar, H. Garse, M. Vij, V. Kadam, Carbon nanotubes and its applications: a review, Asian Journal of Pharmaceutical and Clinical Research 2 (4) (2009) 17–27.

[2] M. F. De Volder, S. H. Tawfick, R. H. Baughman, A. J. Hart, Carbon nanotubes: present and future commercial applications, science 339 (6119) (2013) 535–539.

[3] A. Gangele, C. S. Sharma, A. K. Pandey, Synthesis of patterned vertically aligned carbon nanotubes by pecvd using different growth techniques: a review, Journal of nanoscience and nanotechnology 17 (4) (2017) 2256–2273.

[4] H. Qi, K. Teo, K. Lau, M. Boyce, W. Milne, J. Robertson, K. Gleason, Determination of mechanical properties of carbon nanotubes and vertically aligned carbon nanotube forests using nanoindentation, Journal of the Mechanics and Physics of Solids 51 (11) (2003) 2213–2237.

[5] C. Daraio, V. F. Nesterenko, S. Jin, W. Wang, A. M. Rao, Impact response by a foamlike forest of coiled carbon nanotubes, Journal of applied physics 100 (6) (2006) 064309.

[6] E. H. Teo, W. K. Yung, D. H. Chua, B. Tay, A carbon nanomattress: A new nanosystem with intrinsic, tunable, damping properties, Advanced Materials 19 (19) (2007) 2941–2945.

[7] S. D. Mesarovic, C. McCarter, D. Bahr, H. Radhakrishnan, R. Richards, C. Richards, D. McClain, J. Jiao, Mechanical behavior of a carbon nanotube turf, Scripta materialia 56 (2) (2007) 157–160.

[8] S. Pathak, Z. G. Cambaz, S. R. Kalidindi, J. G. Swadener, Y. Gogotsi, Viscoelasticity and high buckling stress of dense carbon nanotube brushes, Carbon 47 (8) (2009) 1969–1976.

[9] P. Zhang, Y. Huang, P. Geubelle, P. Klein, K. Hwang, The elastic modulus of single-wall carbon nanotubes: a continuum analysis incorporating interatomic potentials, International Journal of Solids and Structures 39 (13) (2002) 3893–3906.

[10] E. T. Thostenson, T.-W. Chou, On the elastic properties of carbon nanotube-based composites: modelling and characterization, Journal of Physics D: Applied Physics 36 (5) (2003) 573.

[11] C. Li, T.-W. Chou, A structural mechanics approach for the analysis of carbon nanotubes, International Journal of Solids and Structures 40 (10) (2003) 2487–2499.

[12] C. Li, T.-W. Chou, Modeling of elastic buckling of carbon nanotubes by molecular structural mechanics approach, Mechanics of Materials 36 (11) (2004) 1047–1055.

[13] C. Wang, Y. Zhang, C. Wang, V. Tan, Buckling of carbon nanotubes: a literature survey, Journal of nanoscience and nanotechnology 7 (12) (2007) 4221–4247.

[14] H. Shima, Buckling of carbon nanotubes: a state of the art review, Materials 5 (1) (2011) 47–84.

[15] C. Ru, Column buckling of multiwalled carbon nanotubes with interlayer radial displacements, Physical Review B 62 (24) (2000) 16962.

[16] M. J. Buehler, Y. Kong, H. Gao, Deformation mechanisms of very long single-wall carbon nanotubes subject to compressive loading, Journal of Engineering Materials and Technology 126 (3) (2004) 245–249.

[17] Y. Li, H.-i. Kim, B. Wei, J. Kang, J.-b. Choi, J.-D. Nam, J. Suhr, Understanding the nanoscale local buckling behavior of vertically aligned mwcnt arrays with van der waals interactions, Nanoscale 7 (34) (2015) 14299–14304.

[18] B. I. Yakobson, C. Brabec, J. Bernholc, Nanomechanics of carbon tubes: instabilities beyond linear response, Physical review letters 76 (14) (1996) 2511.

[19] C. Ru, Elastic buckling of single-walled carbon nanotube ropes under high pressure, Physical Review B 62 (15) (2000) 10405.

[20] C. Ru, Axially compressed buckling of a doublewalled carbon nanotube embedded in an elastic medium, Journal of the Mechanics and Physics of Solids 49 (6) (2001) 1265–1279.

[21] C.-L. Zhang, H.-S. Shen, Thermal buckling of initially compressed single-walled carbon nanotubes by molecular dynamics simulation, Carbon 45 (13) (2007) 2614–2620.

[22] T. Murmu, S. Pradhan, Buckling analysis of a single-walled carbon nanotube embedded in an elastic medium based on nonlocal elasticity and timoshenko beam theory and using dqm, Physica E: Low-dimensional Systems and Nanostructures 41 (7) (2009) 1232–1239.

[23] X. Guo, A. Y. Leung, X. He, H. Jiang, Y. Huang, Bending buckling of single-walled carbon nanotubes by atomic-scale finite element, Composites Part B: Engineering 39 (1) (2008) 202–208.

[24] X. Yao, Q. Han, H. Xin, Bending buckling behaviors of single-and multi-walled carbon nanotubes, Computational Materials Science 43 (4) (2008) 579–590.

[25] A. Gangele, A. K. Pandey, Elastic and fracture characteristics of graphene-silicon nanosheet composites using nonlinear finite element method, International Journal of Mechanical Sciences 142-143 (2018) 491 – 501. doi:https://doi.org/10.1016/j.ijmecsci.2018.05.012.
URL http://www.sciencedirect.com/science/article/pii/S0020740318301036

[26] K. Tserpes, P. Papanikos, Finite element modeling of single-walled carbon nanotubes, Composites Part B: Engineering 36 (5) (2005) 468–477.

[27] A. Kalamkarov, A. Georgiades, S. Rokkam, V. Veedu, M. Ghasemi-Nejhad, Analytical and numerical techniques to predict carbon nanotubes properties, International journal of Solids and Structures 43 (22) (2006) 6832–6854.

[28] E. Mohammadpour, M. Awang, Nonlinear finite-element modeling of graphene and single-and multi-walled carbon nanotubes under axial tension, Applied Physics A 106 (3) (2012) 581–588.

[29] MATLAB, version 7.10.0 (R2010a), The MathWorks Inc., Natick, Massachusetts, 2010.

[30] ANSYS Mechanical APDL 15.0–Basic Analysis Guide (2013).

[31] C. Li, T.-W. Chou, Elastic moduli of multi-walled carbon nanotubes and the effect of van der waals forces, Composites Science and Technology 63 (11) (2003) 1517–1524.

[32] W. Chen, E. Lui, Structural Stability: Theory and Implementation, PTR Prentice Hall, 1987.
URL https://books.google.co.in/books?id=T98ePwAACAAJ

[33] Q. Wang, V. Varadan, S. Quek, Small scale effect on elastic buckling of carbon nanotubes with nonlocal continuum models, Physics Letters A 357 (2) (2006) 130–135.

[34] S. P. Timoshenko, J. M. Gere, Theory of elastic stability, Courier Corporation, 2009.

[35] C. P. Deck, J. Flowers, G. S. McKee, K. Vecchio, Mechanical behavior of ultralong multiwalled carbon nanotube mats, Journal of Applied Physics 101 (2) (2007) 023512.

[36] T. Tong, Y. Zhao, L. Delzeit, A. Kashani, M. Meyyappan, A. Majumdar, Height independent compressive modulus of vertically aligned carbon nanotube arrays, Nano letters 8 (2) (2008) 511–515.

[37] A. Zbib, S. D. Mesarovic, E. Lilleodden, D. McClain, J. Jiao, D. Bahr, The coordinated buckling of carbon nanotube turfs under uniform compression, Nanotechnology 19 (17) (2008) 175704.

[38] S. B. Hutchens, L. J. Hall, J. R. Greer, In situ mechanical testing reveals periodic buckle nucleation and propagation in carbon nanotube bundles, Advanced Functional Materials 20 (14) (2010) 2338–2346.

[39] N. Hu, K. Nunoya, D. Pan, T. Okabe, H. Fukunaga, Prediction of buckling characteristics of carbon nanotubes, International Journal of Solids and Structures 44 (20) (2007) 6535–6550.

[40] K. Dilrukshi, M. Dewapriya, U. Puswewala, Size dependency and potential field influence on deriving mechanical properties of carbon nanotubes using molecular dynamics, Theoretical and Applied Mechanics Letters 5 (4) (2015) 167–172.

[41] M. Meo, M. Rossi, Prediction of youngs modulus of single wall carbon nanotubes by molecular-mechanics based finite element modelling, Composites Science and Technology 66 (11-12) (2006) 1597–1605.

[42] E. Mohammadpour, M. Awang, Predicting the nonlinear tensile behavior of carbon nanotubes using finite element simulation, Applied Physics A 104 (2) (2011) 609–614.

[43] R. Ansari, S. Sahmani, H. Rouhi, Rayleigh–ritz axial buckling analysis of single-walled carbon nanotubes with different boundary conditions, Physics Letters A 375 (9) (2011) 1255–1263.

[44] Y.-G. Sun, X.-H. Yao, Y.-J. Liang, Q. Han, Nonlocal beam model for axial buckling of carbon nanotubes with surface effect, EPL (Europhysics Letters) 99 (5) (2012) 56007.